

# Bondbreaking in PMMA Resists in e-Beam Lithography

DELFT UNIVERSITY OF TECHNOLOGY

BACHELOR END PROJECT

*Mels Habold*

4493508

TNDO 18-10

TECHNICAL UNIVERSITY DELFT

supervisor

Dr. C.W. HAGEN

Supervisory Committee

Dr. J.P. HOOGENBOOM

Kerim Arat MSc.

Luc van Kessel MSc.

## **Abstract**

In electron beam lithography, energy deposition models based on the transferred energy from inelastic scattering processes are commonly used as a method to get an indication of the pattern drawn inside the resist. This method assumes the deposited energy to be proportional to the number of broken bonds per unit volume, giving clear indication to the exposed areas inside the resist.

In this bachelor project, bondbreaking processes for poly-methylmethacrylate (PMMA) resists have been researched. Starting from main-chain scissions as an indication of the exposed areas of the resists, a bondbreaking model based on classical scattering processes has been developed. Both the bondbreaking model and the inelastic energy deposition model has been investigated by comparing them to some different models. These comparisons were made by looking at the locations of the broken bonds, the fraction of bonds broken and by investigating the resulting backscatter yield.

It can be concluded that using bondbreaking as a separate model has no advantage over using the inelastic energy deposition model. Furthermore, it can be concluded that bondbreaking should be part of the (dielectric function-based) inelastic model.

In further research, it would be interesting to look at how bondbreaking can be implemented as part of the inelastic scattering model. For this, it would be interesting to do a deeper research into the quantum mechanical aspects of bondbreaking as well as to investigate it from a more chemical point of view.

# Contents

<b>1</b>	<b>Introduction</b>	<b>2</b>
<b>2</b>	<b>The Material: PMMA</b>	<b>4</b>
<b>3</b>	<b>Theory</b>	<b>7</b>
3.1	Energy transfer . . . . .	8
3.2	Scattering angles . . . . .	10
3.3	Mean Free Path . . . . .	11
3.4	The Simulation . . . . .	13
<b>4</b>	<b>Results</b>	<b>15</b>
4.1	The Models . . . . .	15
4.2	Data Comparison . . . . .	16
4.2.1	The Radial Histograms . . . . .	16
4.2.2	The Fraction on Scattering Events . . . . .	24
4.2.3	Electron Yield . . . . .	26
4.2.4	Independent Processes . . . . .	29
4.2.5	Maximum Number of Broken Bonds . . . . .	29
<b>5</b>	<b>Discussion and Conclusion</b>	<b>30</b>
5.1	Theory Analysis . . . . .	30
5.2	Results Analysis . . . . .	31
5.3	Recommomdations . . . . .	32
5.4	Conclusion . . . . .	32
<b>A</b>	<b>Assumptions of the model</b>	<b>34</b>

# 1 | Introduction

In electron beam (e-beam) lithography, a beam of high energy electrons (10 to 100 keV<sup>[1]</sup>) is fired at a substrate with a resist on top of it. When being exposed to these high energy electrons, the resist layer, which is usually less than a 100 nanometers thick, changes solubility. In positive tone e-beam lithography, the resist is made soluble after being exposed to a sufficiently high dose of high energy electrons. Often, these doses lie around the 150  $\mu\text{C}/\text{cm}^2$ . After the areas of the resists have been made soluble, they are removed using developers. The remaining resist protects the substrate against further processing steps, such as etching, which are the steps responsible for drawing structures in the substrate.

When writing structures at a sub 10 nm level<sup>[2,3]</sup>, or when using smaller doses of electrons, the written structures in the resist become uncertain due to the random scattering of electrons throughout the resist. To get a better understanding of the uncertainty this proximity effect imposes on the structures written onto the substrate in e-beam lithography, many models have been developed to simulate the stochastic paths the electrons take inside the resist.

The first models that tried to estimate e-beam scattering inside resists were based on elastic scattering and the stopping power. These models used a Monte Carlo simulation to simulate the paths the electrons take inside the resist and used the stopping power as an indication of the energy loss per particle, which was assumed to be proportional to the solubility change of exposed areas inside the resist.

These models only used elastic scattering events as scattering mechanisms and used the stopping power to make the electrons lose energy continuously. Both assumption were quite wrong as the electron loses energy due to discrete inelastic scattering events, which plays a big role in modern models. These energy deposition models use the energy transferred due to inelastic scattering events as an indication of the exposed areas of the resist. These models also encompassed a more theoretically correct way to describe the creation of secondary electrons.

Most scattering models are based on cross sections, which are an indication to the closest distance two particles can have without having a notable interaction. Take for example two billiard balls. The cross section is related to the sum of the radii of both balls, meaning that if the distance between the two balls is bigger than the sum of the two radii, no scattering will take place as the two billiard balls do not collide. It is important to note that the probability of scattering the two billiard balls is also dependent on the relative motion the balls have to each other. Therefore, the cross section is also dependent on the kinetic energy of both particles.

When using electrons instead of billiard balls, electromagnetic forces and quantum mechanical effects play the leading role in the cross section. In 1965, Gryzinski already made great improvements on inelastic processes by introducing his two beam collision theory for coulomb interaction Gryzinski, M (1965)<sup>[4,5]</sup>, in which he also derived his ionization cross section. Vriens quickly proposed a few improvements in 1966 and introduced his cross sections<sup>[6]</sup>.

In the energy deposition model, the deposited energy is assumed to be an indication to the areas of the resist which are made soluble. In fact, it is more likely that bondbreaking is the cause of the change of solubility. In this paper, we will therefore investigate bondbreaking and how it could be implemented together with other scattering processes in order to get a clear view on the areas of the resists that are exposed.

We will follow the framework set out by Wu, B. (2001)<sup>[7]</sup>, which uses Vriens' cross section to approximate the effects of exposure. We use this cross section to calculate the mean free path (MFP) of the bondbreaking event, which we can use to draw a free path length from an exponential distribution. This free path length gives us an indication of the probability that the bondbreaking event will happen, which seems intuitive because events with a smaller MFP should happen more often.

The MFP, together with the transferred energy and the scattering angle, is used to make our own bondbreaking model. This model will be implemented in a simulation package which already includes Penn's inelastic scattering model<sup>[8]</sup>, which is based on the dielectric function, and Motts elastic model<sup>[9]</sup>.

As time is limited, we will only focus our theory on the resist called Poly-Methyl Methacrylate (PMMA), a polymer that has very little chemical interactions, which makes it great to base the model on as it is also a popular resist for e-beam lithography and it can be easily extended to encompass other polymers as well.

In chapter 2, PMMA and the material properties of interest are introduced. In chapter 3, the theory and the mathematics behind bondbreaking is developed and implemented in the simulation package. In chapter 4 we will compare our model with some other models. This comparison will be done by looking at the locations of the broken bonds, the fraction of bondbreaking events and by looking at the electron yield. In chapter 5, both the theory behind the model from chapter 3 and the comparisons from chapter 4 will be discussed and a conclusion is given. Besides that, a few recommendations for further research are made.

The list of assumptions made in this report can be found in appendix A.

## 2 | The Material: PMMA

Poly-Methyl Methacrylate, or PMMA in short, is a long chain of monomers of Methyl Methacrylate. Figure 2.1 shows the structure of one PMMA monomer.

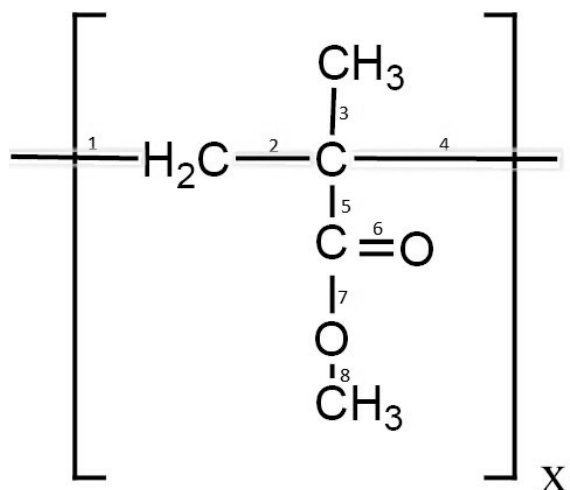


**Figure 2.1:** A structural graphic of one PMMA monomer<sup>[10]</sup>. The C-C bonds that take part in main-chain scissions (with number 1, 2 and 4) are highlighted.

PMMA is a widely used resist which is able to act both as a positive- and- negative-tone resist. The positive-tone means that, when exposed to electrons, the material becomes soluble. When using a high dose of low energy electrons, the material can also become less soluble due to cross linking <sup>1</sup> (from Carbaugh, D. (2016)<sup>[11]</sup>), which are the characteristics of a negative-tone resist.

In this report, the breaking of bonds resulting in a change in solubility of PMMA is investigated. Because we are mostly interested in the more commonly used high energy electron beams, the effects of reconfiguration of the polymers due to cross linking will be neglected. This however also means that the effects of cross linking due to low energy secondary electrons resulting from inelastic scattering events are ignored.

---

<sup>1</sup>Cross linking is not of interest in this report but is explained in<sup>[1]</sup> Figure 16.

## Physical and Chemical Properties

Table 2.1 contains the physical and chemical properties of interest of PMMA. It can be seen that the average amount of monomers per polymer (or degree of polymerization) varies largely. Since these are average numbers, it can be assumed that a polymer chain has a great variation in length, which means that no quantitative indication to the maximum amount of broken bonds per chain or the number of bonds that need to be broken per chain to make PMMA soluble can be given. It is however interesting to look at the number density, which lies at 7.05 monomers per cubic nanometer and gives a clear indication on the maximum amount of bonds that can be broken per cubic nanometer.

**Table 2.1:** Physical and chemical properties of interest of PMMA.

Property	Sign	Value
Density of a monomer at room temperature	$R_{PMMA}$	1.18 g/cm <sup>3</sup> [12]
Molar weight of a monomer	$M_0$	100.121 g/mol[12]
Number average molar mass	$M_n$	10,000 to 1000,000 g/mol[11]
Molar Volume	$\frac{M_0}{R_{PMMA}} V_M$	85.4 cm <sup>3</sup> /mol
Number density of the monomers	$V_M^{-1}$	7.05 monomers/nm <sup>3</sup>
Degree of polymerization	$\frac{M_n}{M_0}$	100 to 10,000 monomers per polymer

## Atoms and Bonds

Not every atom can make the same amount of bonds. The number of bonds an atom can make is both dependent on the number of valence electrons the atom has and the number of valence electrons the atom is willing to accept. The amount of bonds and valence electrons of the different atoms in PMMA are given in table 2.2.

**Table 2.2:** Bonds and valence electrons of each atom in PMMA.

Atom	Sign	Number of valence electrons	Number of bonds
Carbon	C	4	4
Oxygen	O	6	2
Hydrogen	H	1	1

There are, if one of the bonds that connects the monomer to its neighbour is excluded, a total of 16 bonds (counting the C=O as 2) and 40 valence electrons per monomer.

The bonds of interest are the main-chain bonds (the highlighted bonds indicated with the numbers 1, 2 and 4 in figure 2.1). This single covalent bond in between two carbon atoms in the main chain is the backbone of the polymer and has a binding energy of 4.9eV Wu, B. (2001)<sup>[7]2</sup>. Based on Aktary, M (2006)<sup>[13]</sup> and Stepanova, M. (2010)<sup>[14]</sup>, it can be assumed that only inelastic collisions with these main-chain C-C bonds will result in main-chain scissions, ignoring any possible indirect chemical reactions that can result

<sup>2</sup>We cannot accurately calculate the binding strength of outer shell electrons. Aktary, M. (2006)<sup>[13]</sup> tells us the binding energy is in between 3.3 and 3.6eV, Wu, B. (2001)<sup>[7]</sup> says its 4.9eV. Since we base our report on that of Wu, we will assume the 4.9eV to be the right binding energy.

in main-chain scissions. It is also assumed that only main-chain scissions result in a change in solubility of PMMA.

## 3 | Theory

The bondbreaking mechanism used in the model of this report will be based on Wu's report<sup>[7]</sup>. As shown in figure 3.1, an incident primary electron with kinetic energy  $E$  breaks a covalent bond by hitting one of the valence electrons of the covalent bond out of orbit. This covalent electron will become a secondary electron that travels within the conduction band with an angle  $\beta$  to the original direction of the primary. After collision, the primary electron will have lost energy  $\omega$  and will travel further in the conduction band with an angle  $\alpha$  to the original direction. It is assumed that the binding energy  $U$  disappears into repulsion energy so that the distance between the atoms increases slightly after a bond is broken. This extra inter-atomic distance will be assumed infinitely small for PMMA, rendering the binding energy  $U$  negligible. It is also assumed that only the collision with covalent electrons will result in a broken bond, ignoring possible inner shell electron excitations<sup>1</sup>, electron trapping and other physical processes resulting in the breaking of a bond.

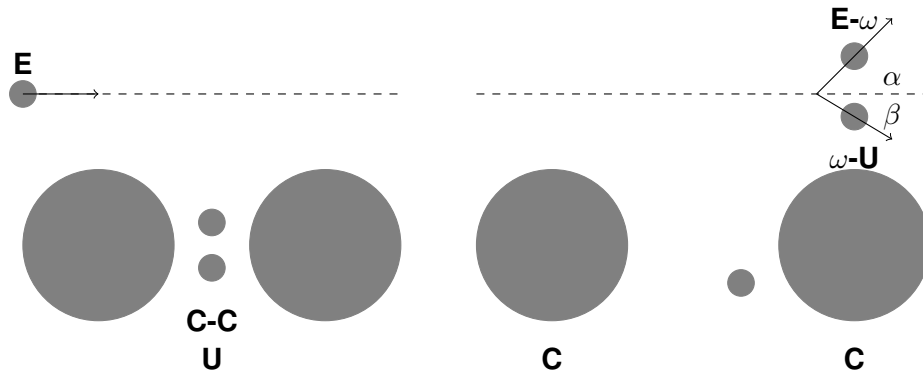


**Figure 3.1:** (left) An incoming electron with energy  $E$  and a carbon-carbon bond with binding energy  $U$ . (right) The electron breaks the bond by hitting one electron out of orbit. The transferred energy is  $\omega$  and the secondary electron pays the bond energy of the broken bond.

In chapter 3.1, Vriens' differential cross section<sup>[6]</sup> is used to calculate the energy transfer  $\omega$  using the primary energy  $E$ . Using both the primary energy  $E$  and the transferred energy  $\omega$ , the polar scattering angles  $\alpha$  and  $\beta$  are calculated in chapter 3.2. The az-

<sup>1</sup>[15] already shows that inner shell electron excitations can lead to the ionization of various groups. Most of these excitations are adjacent molecules, but still a significant fraction of inner shell excitations lead to the ionization of main chain carbon groups, resulting in main-chain scissions.

imuthal scattering angle (the angle in the plane transverse to the direction of motion of the incident particle) is assumed to be uniformly distributed on the interval  $[0, 2\pi]$ . From Vriens' differential cross section, the primary energy  $E$  and the transferred energy  $\omega$ , the attenuation coefficient is also calculated in chapter 3.3.

### 3.1 Energy transfer

The energy loss distribution (ELD) is a cumulative distribution function that calculates the transferred energy  $\omega$  for a certain energy  $E$  and binding energy  $U$ . A cumulative distribution function (like the ELD) is calculated by taking the area under the probability density function from minus infinity to  $\omega$ ,

$$F_\Omega(\omega) = \frac{1}{\sigma_{\text{tot}}} \int_{-\infty}^{\omega} \frac{d\sigma}{d\omega'}(E, \omega', U) d\omega' \quad (3.1)$$

In which  $\frac{d\sigma}{d\omega}$  is the differential cross section and  $\sigma_{\text{tot}}$  is the total cross section used to normalize the ELD. Because the differential cross section is proportional to the probability a primary electron with energy  $E$  has to transferring an energy  $\omega$ , it is used here as a probability density function.

The ELD will be derived by first introducing the differential cross section. Further on, the boundaries which will be used to calculate the total cross section will be determined. At the end, the differential cross section and the total cross section will be used in equation (3.1) to calculate the ELD.

#### Differential Cross Section

In 1965, Gryzinski made great improvements on inelastic theories by introducing his two beam collision theory Gryzinski, M (1965)<sup>[4,5]</sup>. This theory used classical scattering mechanisms together with Coulomb interaction to calculate how two beams of electrons would scatter from each other. Gryzinski further extended his theory by introducing his differential ionization cross section, which included both inner shell and outer shell electron excitations. Shortly after Gryzinski posted his papers, Vriens made some big improvements and made his own differential ionization cross section Vriens, L (1966)<sup>[16]</sup>.

Wu, B. (2001)<sup>[7]</sup> used Vriens' differential ionization cross section for outer shell electron excitations to base his theory on bondbreaking on. This differential cross section is given in equation (3.2) and can be found in Wu (page 1) or Vriens<sup>[16]</sup> (page 16),

$$\begin{aligned} \frac{d\sigma}{d\omega} &= \frac{1}{(4\pi\epsilon_0)^2} \frac{\pi e^4}{E + 2U} \left[ \left\{ \frac{1}{\omega^2} + \frac{4U}{3\omega^3} \right\} + \left\{ \frac{1}{(E + U - \omega)^2} \right. \right. \\ &\quad \left. \left. + \frac{4U}{3(E + U - \omega)^3} \right\} - \frac{\Phi}{\omega(E + U - \omega)} \right] \\ \Phi &= \cos \left( -\sqrt{\frac{R_y}{E + U}} \log \frac{U}{E} \right) \end{aligned} \quad (3.2)$$

In which  $R_y$  is the Rydberg energy (13.6eV),  $\epsilon_0$  the permittivity of vacuum and  $e$  the electron charge. A factor  $(4\pi\epsilon_0)^{-2}$  is introduced to make up for using SI units instead of Gaussian units.

### Implementing Vriens' differential cross section

The simulation package already has Penn's inelastic scattering model and Mott's elastic scattering model in it. To investigate if bondbreaking is already part of Penn's inelastic scattering model, we will assume that it is not and check if it renders realistic results. This means that the bondbreaking model derived in this report based on Vriens' differential cross section will be assumed to be a process independent of Penn's inelastic scattering model.

### Boundaries

It can be seen that equation (3.2) is symmetric on the interval  $\Omega = [U, E]$ . The lower boundary is equal to the binding energy  $U$  as it is assumed that a primary electron will be unable to break a bond if the transferred energy is lower than the binding energy. The upper boundary is chosen because the primary energy cannot lose more than its own energy.

Because the differential cross section is symmetric, the total space  $\Omega$  can be split into two regions of the same size  $\Omega_1 = [U, \frac{E+U}{2}]$  and  $\Omega_2 = [\frac{E+U}{2}, E]$ . This symmetry gives the particles an interesting aspect called indistinguishability, which means that for every transferred energy  $\omega_1$  inside region  $\Omega_1$ , there exists an  $\omega_2$  inside region  $\Omega_2$  equal to  $\omega_1$ . This means that each possible energy configuration can come from either  $\Omega_1$  or  $\Omega_2$ .

**Table 3.1:** An illustration showing the interchangeability of the primary and secondary electrons.

transfer	primary	secondary
$\omega$	$E-\omega$	$\omega-U$
$E$	0	$E-U$
$U$	$E-U$	0
$\frac{E+U}{2}$	$\frac{E-U}{2}$	$\frac{E-U}{2}$

As the two particles are indistinguishable, Vriens, L.(1966)<sup>[6]</sup> only uses the interval  $\Omega_1 = [U, \frac{E+U}{2}]$ , with  $\omega \in \Omega_1$ , to render correct results.

### Total Cross section

With the new boundaries,  $\sigma_{tot}$  can be calculated from equation (3.2),

$$\sigma_{tot} = \frac{1}{(4\pi\epsilon_0)^2} \frac{\pi e^4}{E+2U} \left[ \frac{5}{3U} - \frac{1}{E} - \frac{2U}{3E^2} - \frac{\Phi}{U+E} \log \left| \frac{E}{U} \right| \right] \quad (3.3)$$

## Energy Loss Distribution

Now, the ELD can be calculated from equations (3.1) and (3.2),

$$F_{\Omega_1}(\omega) = \frac{1}{\sigma_{\text{tot}}} \int_U^\omega \frac{d\sigma}{d\omega'}(E, \omega', U) d\omega' \quad (3.4)$$

$$\begin{aligned} F_{\Omega_1}(\omega) = & \frac{1}{\sigma_{\text{tot}}} \frac{1}{(4\pi\epsilon_0)^2} \frac{\pi e^4}{E + 2U} \left[ \frac{5}{3U} - \frac{1}{\omega} - \frac{2U}{3\omega^2} \right. \\ & + \frac{1}{E + U - \omega} + \frac{2U}{3(E + U - \omega)^2} - \frac{1}{E} - \frac{2U}{3E^2} \\ & \left. + \frac{\Phi}{E + U} \log \left( \frac{(E + U - \omega)U}{E\omega} \right) \right] \end{aligned} \quad (3.5)$$

A simulation is only able to draw (semi-)random variables from a uniform random distribution. In order to draw the random variable  $\omega$  that follows the distribution  $F_\Omega$  from a uniform random number  $u$ , the inverse cumulative distribution function (ICDF) needs to be solved,

$$\begin{aligned} F_\Omega(\omega) &= u \\ \omega &= F_\Omega^{-1}(u) \end{aligned} \quad (3.6)$$

Using equation (3.5) in equation (3.6) is impossible to solve analytically. Therefore a numerical tool called cstool<sup>[17]</sup> (short for cross section tool), which is able to solve our ICDF and export it into a table, will be used.

## 3.2 Scattering angles

The polar angles by which the two electrons are scattered can be described by Verduin, T. (2017)<sup>[18]</sup> page 80,

$$\begin{aligned} \cos \alpha &\approx \sqrt{1 - \frac{\omega}{E}} \\ \cos \beta &\approx \sqrt{\frac{\omega}{E}} \end{aligned} \quad (3.7)$$

In which any relativistic effects are ignored and the conservation of momentum in both the perpendicular and tangential directions is assumed. The derivation of equation 3.7 follows classical inelastic collision mechanics. Equation (3.7) holds only for free electrons but since one of these electrons is bound, page 84 of Verduin corrects the energies of equation (3.7) into:

$$\begin{aligned} E &\rightarrow E - E_F + 2U \\ \omega &\rightarrow \omega + U \end{aligned}$$

In which  $E_F$  is the Fermi energy of the polymer, which is hard to calculate for insulators like PMMA but can be described for metals.

The Fermi energy of a metal is inside of the conduction band of that metal. When an electron enters the conduction band, it gains an extra energy so that it is able to enter the lowest available state in the conduction band. In this report, this effect is also assumed for PMMA. Furthermore, the electrons at the bottom of the conduction band in PMMA are assumed to be free but not moving, which means the Fermi energy is equal to zero.

With this information, equation (3.7) becomes,

$$\begin{aligned}\cos \alpha^* &\approx \sqrt{1 - \frac{\omega + U}{E + 2U}} \\ \cos \beta^* &\approx \sqrt{\frac{\omega + U}{E + 2U}}\end{aligned}\quad (3.8)$$

### 3.3 Mean Free Path

The inverse mean free path (IMFP), or attenuation coefficient, can be calculated using,

$$\mu^{tot} = N \cdot \sigma_{tot}(E, \omega, U) \quad (3.9)$$

With  $\mu^{tot}$  the total IMFP,  $N$  the number density of the particles or molecules of interest,  $U$  the average binding energy and  $\sigma_{tot}$  the total cross section from equation (3.3).

Since only inelastic collisions with valence electrons involved in main-chain C-C bonds in PMMA are of interest, the number density of the main-chain C-C bonds found in chapter 2 can be used to calculate the IMFP. The number density of PMMA monomers is  $7.05 \text{ nm}^{-3}$ , and two C-C bonds (so 4 valence electrons) per monomer take part in the main-chain C-C bonds, so there is a total of  $N_{\text{valence,C-C}}=28.2$  valence electrons per cubic nanometer. The IMFP now is equal to,

$$\mu_{C-C}^{tot}(E) = \frac{28.2[\text{nm}^{-3}]}{(4\pi\epsilon_0)^2} \frac{\pi e^4}{E + 2U} \left[ \frac{5}{3U} - \frac{1}{E} - \frac{2U}{3E^2} - \frac{\Phi}{U+E} \log \left| \frac{E}{U} \right| \right] \quad (3.10)$$

Vriens' cross section is based on all the bonds in a monomer. In this model however, the cross section is only used for main-chain C-C bonds, which only make up one-tenth of all bonds in the monomer. This means that having a number density of 28.2 electrons per cubic nanometer completely ignores the adjacent bonds in the monomer. Normally, ignoring these adjacent bonds wouldn't matter as they would be part of the normal inelastic scattering process, but as we assumed our bondbreaking model to be independent of Penn's inelastic model, this is not the case.

Vriens' differential cross section should therefore be implemented with the adjacent bonds included. We estimate this differential cross section to be the same as described in (3.10), but than with a number density 10 times larger than it already is to make it encompass the non main-chain bonds. This cross section will be discussed in the results.

## Mean Free Path Analysis

For a clear comparison between the scattering processes used in the simulation, the mean free paths of each model is given in figure 3.2.

*Penn's inelastic model*<sup>[8]</sup>, is the MFP on which the inelastic scattering process of the simulation package is based upon. This model is based on the dielectric function and because the complete calculations are quite complicated they can be found in Verduin, T. (2017)<sup>[18]</sup> chapter 3.3: inelastic scattering.

*Vriens' ionization model*<sup>[16]</sup> The mean free path that is calculated in equation (3.10) in this report.

*Mott's Elastic Model*<sup>[18]</sup> For good measure, the elastic scattering process of the simulation package is also compared.

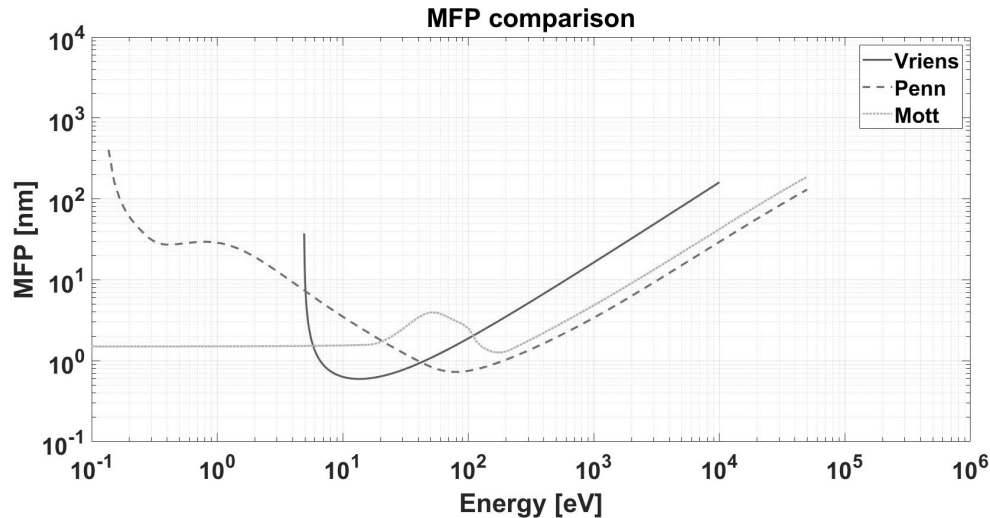


**Figure 3.2:** The Mean Free Path derived from our bondbreaking model (Vriens), Penn's inelastic model and Mott's elastic model. Matlab<sup>[19]</sup> was used to plot these results.

When looking at figure 3.2, we can see that the mean free path of Vriens is bigger than Penn in the higher energy regime, but lower than Penn around 50eV. This would imply that the bondbreaking model as derived in this chapter cannot be a subset of Penn's inelastic model.

This is because if Vriens was part of Penn's model, the MFP of non-Vriens inelastic scattering mechanisms would be calculated using,

$$\frac{1}{\lambda_{\text{Penn, total}}(E)} = \frac{1}{\lambda_{\text{Vriens}}(E)} + \frac{1}{\lambda_{\text{Non-Vriens}}(E)} \quad (3.11)$$

$$\lambda_{\text{Non-Vriens}}(E) = \left[ \frac{1}{\lambda_{\text{Penn, total}}(E)} - \frac{1}{\lambda_{\text{Vriens}}(E)} \right]^{-1} \quad (3.12)$$

If Vriens' MFP would be smaller at a certain energy, that would mean that the non-Vriens scattering mechanisms at that energy would get a negative MFP, which is impossible. It however does not exclude the possibility that Vriens is part of Penn's inelastic

model at higher energies as it exceeds the MFP of Penn, but at lower energies we can conclude Vriens not to be part of Penn's inelastic model.

If we however were to introduce Vriens with a number density 10 times larger to account for all the bonds and not only the main-chain C-C bonds, Vriens' MFP would become lower than Penn at every energy. This would mean that this 'more complete' Vriens model cannot be part of Penn's inelastic model.

Penn's inelastic model could however be part of Vriens model, but as Vriens only describes outer shell excitations, and Penn describes a lot more scattering event (like inner shell excitations, plasmon excitations, general inelastic scattering, etc) it seems unlikely that this is possible.

### 3.4 The Simulation

The previously described bondbreaking model will be implemented into the simulation package which already contains Penn's dielectric based inelastic scattering model and Mott's elastic scattering model.

The simulation uses a Monte Carlo simulation to simulate the paths the electrons take. This means that the simulation iterates between the particles and uses random variables. Each iteration, one scattering event is chosen and executed for the particle of that iteration. This means that the first step would be to chose what scattering event the particle will encounter. This will be done by the next steps:

1. A particle with energy  $E$  and a certain position inside the material is chosen.
2. Inverse mean free paths are calculated for each type of scattering event. ( $\mu_{\text{bondbreaking}}$ ,  $\mu_{\text{inelastic}}$ ,  $\mu_{\text{elastic}}$ )
3. Following the Beer-Lambert Law, the free path lengths are drawn from an exponential distribution using a random number generator.
4. The event with the smallest free path length is chosen to be the event that will happen<sup>2</sup>.

If bondbreaking is the event that is chosen, the next steps will happen:

1. The transferred energy  $\omega$  is drawn from a distribution dependent on  $E$ . The actual distribution is put in a 2D table which is calculated using cstool<sup>[17]</sup> and the equations from section 3.1.
2. The primary electron is scattered with angle  $\alpha^*$  following equations (3.8), a random azimuthal angle is drawn from a Uniform  $(0,2\pi)$  random distribution, travels the distance of the free path length and loses an energy  $\omega \in \Omega_1$ .
3. A secondary particle is rendered with a polar scattering angle  $\beta^*$  from equations (3.8) and a random azimuthal angle drawn from a  $U(0,2\pi)$  random distribution. This particle has energy  $\omega-U$ .

---

<sup>2</sup>This method is equivalent to normal calculations, in which first the total MFP is calculated, then used to normalize the IMFP of each event which is used as a probability that that event will happen.

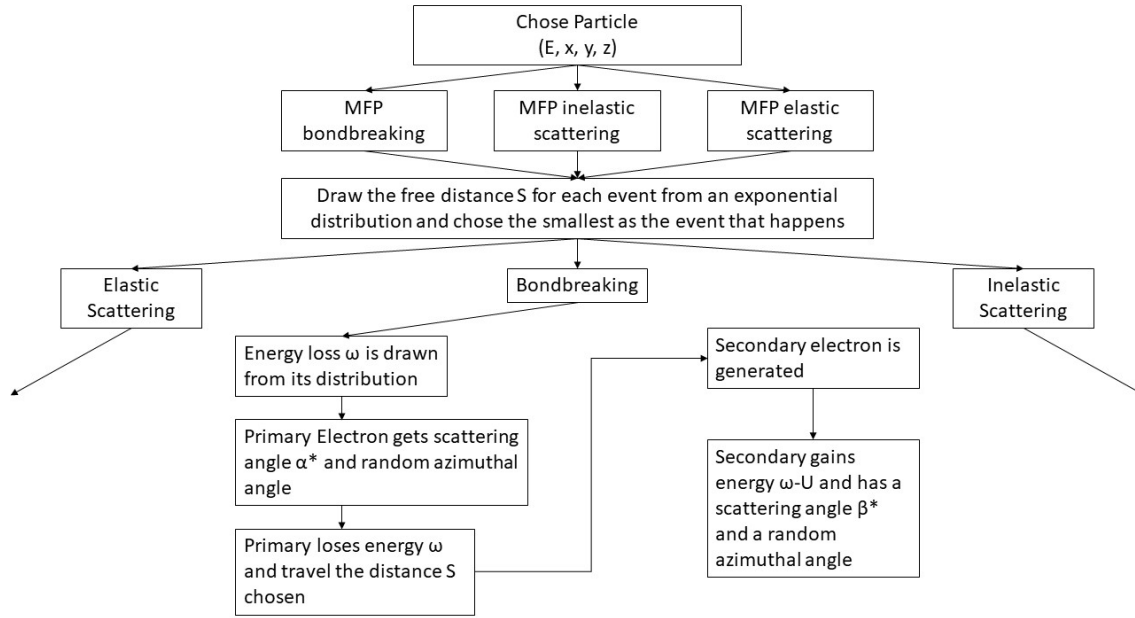


**Figure 3.3:** A diagram for better understanding of the steps the simulation takes. As inelastic scattering and elastic scattering are part of another simulation package, their steps are not shown.

The probability of a main-chain scission event should change during simulations as some of the bonds are already broken. However, since we are mostly interested in the shape of the distribution of main-chain scission events throughout the resist, which should be calculated independently of the dose to make it encompass different scenarios, assuming that the material stays unchanged during simulation actually makes sense.

# 4 | Results

In order to get clear results, we would first like to go over what we want to test:

- Test if the shape of the distribution of our model is realistic.
- Test if our model is in agreement with the energy deposition model.
- Test our Vriens Ionization cross section, on which our model is based, is independent of Penn's inelastic scattering model.
- Test if not more than the 14.1 bonds per cubic nanometer from chapter 3 are broken.

Fist of all, a few models will be introduced in section 4.1. These models will be used to compare the results and assumptions with. In section 4.2, these models will be tested and from it a conclusion is drawn.

## 4.1 The Models

The models we are going to test are:

**Model 1: The Original** This is the model as discussed in the theory of this report. It is based on Vriens' cross section for main-chain C-C bonds which is assumed to be independent on Penn's inelastic model.

**Model 2a: 0.2x Cross section** We would like to test how the results differ when the cross section or number density is changed. Therefore, model 2a will be the model from this report, but with a cross section that is 5 times smaller than the original cross section.

**Model 2b: 0.5x Cross section** Same as model 2a, but now the cross section is divided by 2.

**Model 3: Complete Vriens** This model will be used to test how the bondbreaking model would look if it did not only count main-chain events, but also took the breaking of adjacent bonds into account. In this case, the model is still implemented as an independent process besides Penn's inelastic scattering and Mott's elastic scattering.

To mimic the simulation in which all the bondbreaking mechanisms are taken into account, model 1 is modified so that the number density is 10 times larger, to make it en-

compass all the bonds<sup>1</sup>. Thereafter, only 1 out of 10 bondbreaking events are recorded as actual main-chain scissions. However, trying to make the program encompass all bonds by multiplying the number density by 10 means that effects from the binding energies of different bonds are ignored, but as this model only mimics the complete Vriens model, this is allowed.

**Model 4: Implicit Bondbreaking** Together with model 3, the assumption that Vriens' and Penn's model are independent are put to the test.

Model 4 will mimic a model in which bondbreaking is not an independent process by including bondbreaking in Penn's inelastic scattering model and saying that 1 out of 10 inelastic collisions lead to bonds being broken.

In this case, Vriens' cross section, and the mean free path and the energy loss distribution calculated in this report are also ignored. It is however still important to note that in this model, the scattering angles (equation (3.8)) as derived in chapter 3.2 are still used. Furthermore, the one-out-of-ten probability is still only possible if the energy transfer  $\omega$  is bigger than the binding energy  $U$ , which also means that the generated secondary electron has an energy of  $\omega - U$ . This means that this 4th model is not exactly Penn's inelastic model with bondbreaking recorded in it, but more like an approximation on how bondbreaking could look like if implemented as part of Penn's inelastic model.

**Model 5: Energy deposition** As explained in the introduction of this report, one of the commonly used models to calculate the distribution of exposed areas is the energy deposition model. This model uses the transferred energy per inelastic event as an indication of the areas of the resist that have been made soluble. Model 5 will do the same thing for Penn's inelastic scattering model, and will be used for comparison.

## 4.2 Data Comparison

### 4.2.1 The Radial Histograms

First of all, we would like to look at the distribution each model renders. For this, a 20keV beam consisting of 1e5 electrons is used to simulate scattering in an infinitely deep PMMA layer, which means that no substrate layer is simulated. As most resist layers are not thicker than a 100 nm, only bondbreaking events until a depth of a 100 nm's are investigated.

As the model is symmetric in each direction, we prefer to transform the coordinates of the bondbreaking events into cylindrical coordinates. This radial data is then put into histograms. This radial histogram calculates the density per ring with thickness  $\delta r$  around the z-axis. This means that outer rings have a bigger volume than inner rings, as they have a bigger radius. To counter this effect, each radial bin has to be divided by its volume, which is equal to  $2\pi r \delta r \delta h$  in which  $r$  is the distance in nanometers from the z-axis to the center of the bin and  $\delta h$  is the height of each bin.

---

<sup>1</sup>Bondbreaking in model 1 was only for main-chain bonds which make up a total of one-tenth of all bonds in the PMMA monomer.

Furthermore, we are mostly interested in the effect one electron has on the resist. Therefore, not only will each bin be normalized by its volume but also by the total number of primary electrons used in the simulation. This renders the average number of broken bonds per primary electron per cubic nanometer as a function of the depth and the distance to the z-axis.

As most events happen in the close proximity of the entrance beam, the data is presented with a logarithmic plot. Both the Cross section of the plot, as the radius will be presented on a logarithmic scale.

By using the method described above, we end up with the next radial histograms for the original model (model 1) and model 2a and 2b, which are the same models but with a magnitude of the cross section of 0.2 and 0.5 respectively. The corresponding radial plots are figures 4.1, 4.2 and 4.3.

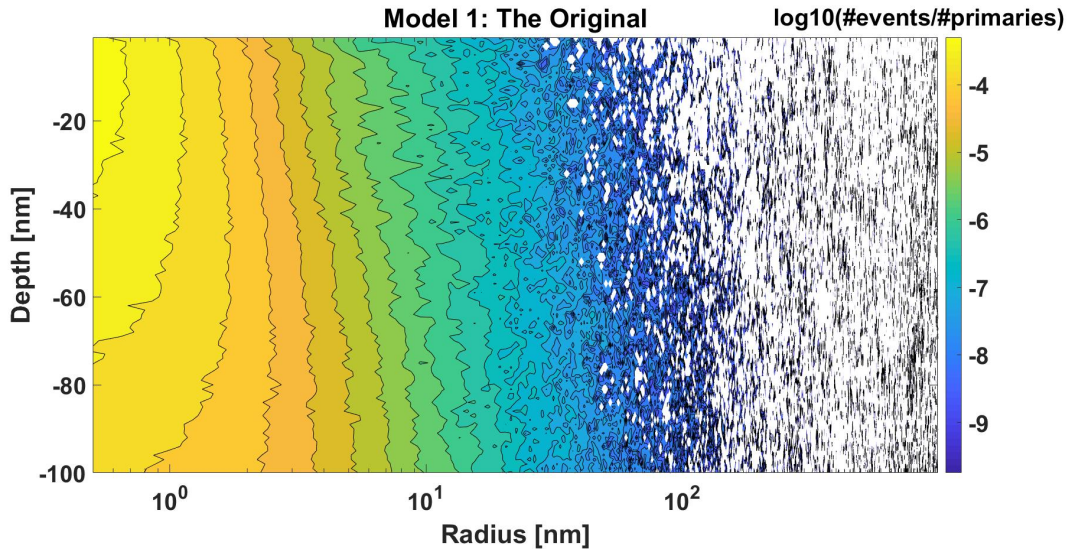


**Figure 4.1:** The normalized bondbreaking effect of our original bondbreaking model (model 1). On the horizontal axis, the radius is given on logarithmic scale, and on the vertical axis, the depth is given. The colorscale is logarithmic.

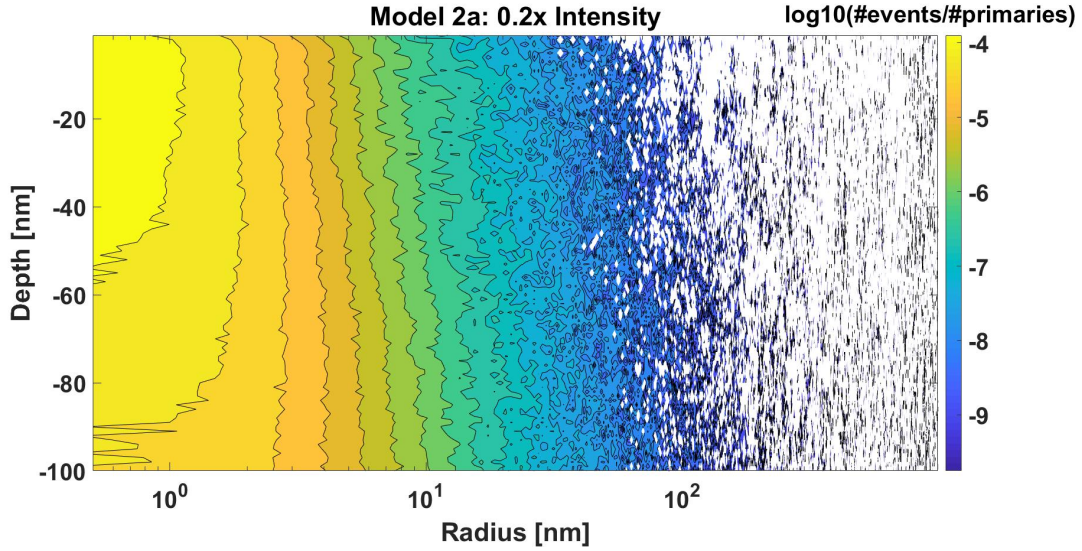


**Figure 4.2:** The normalized bondbreaking effect of our original bondbreaking model with an extra 0.2x (model 2a). On the horizontal axis, the radius is given on logarithmic scale, and on the vertical axis, the depth is given. The colorscale is logarithmic.

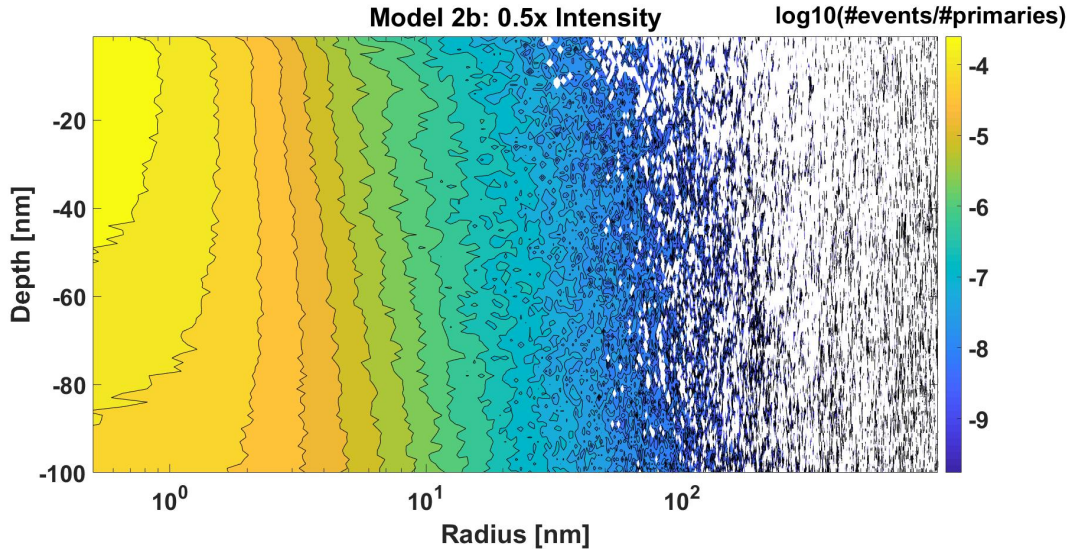


**Figure 4.3:** The normalized bondbreaking effect of our original bondbreaking model with an extra 0.5x (model 2b). On the horizontal axis, the radius is given on logarithmic scale, and on the vertical axis, the depth is given. The colorscale is logarithmic.

To get clear results on the differences between the shapes of the distribution, we look at figures 4.4a and 4.4b. These figures are the logarithmic data from figures 4.1 to 4.3 subtracted from each other. As it is on a logarithmic scale, this is like dividing both intensities. We see that the difference seems to be constant with the logarithmic value of 0.05. This means that in most places, the shape of the distributions are almost equal to

each other. It is however important to note the there seems to be some noise far away from the z-axis and that there seems to be a big spot with the logarithmic value of -0.3 (so the original model is 0.5 times bigger in those positions). These spots are however in parts where the material is mostly untouched by our model, so they are of no interest.

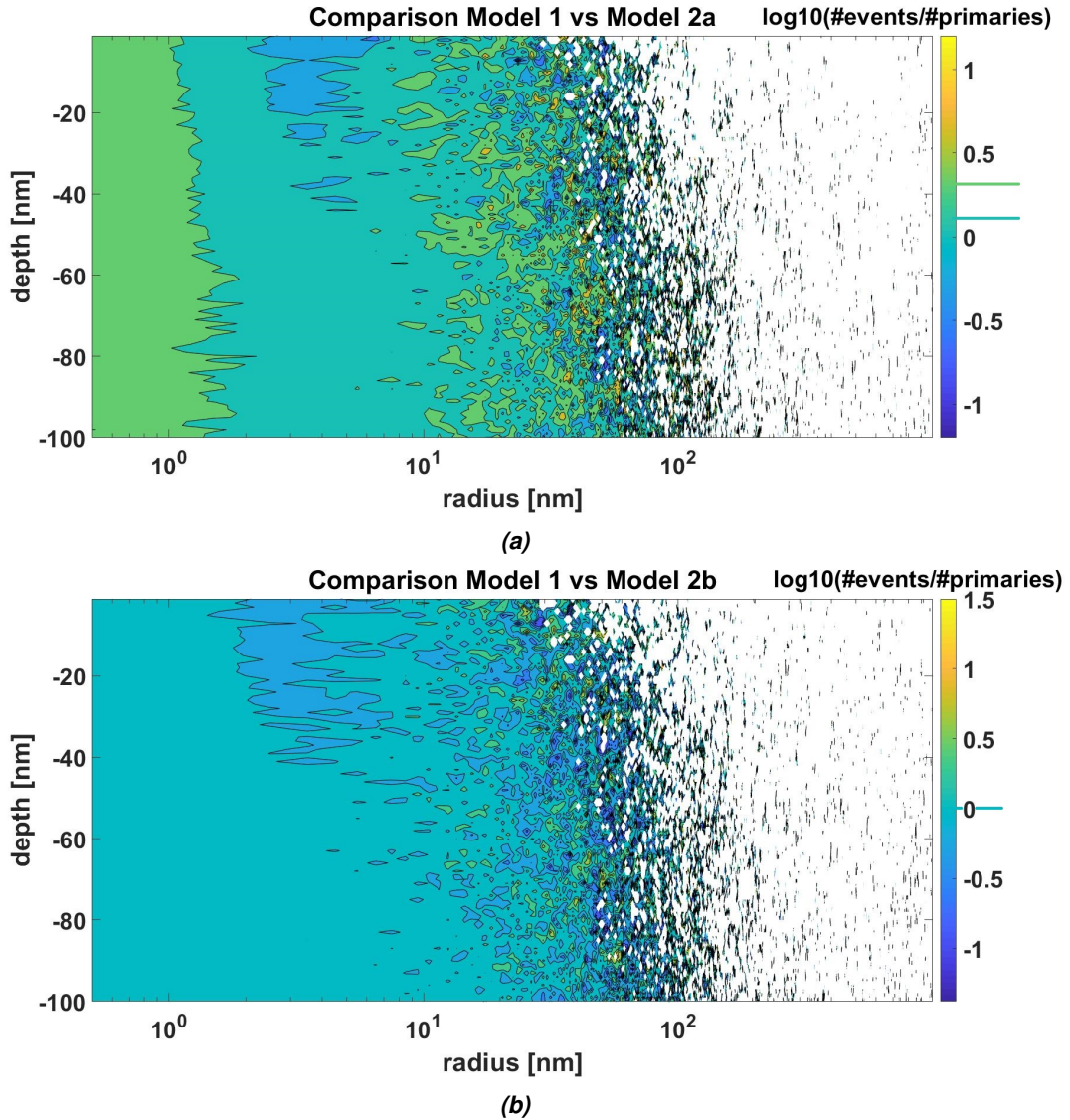


**Figure 4.4:** (a) The difference between figure 4.1 and 4.2. (b) the difference between figure 4.1 and 4.3.

One notable difference however is the big pilar in the middle of figure 4.4a, which indicates that the original model is 2 times bigger in that spot than the 0.2x Cross section model. This tells us that changing the magnitude of the cross section too much will have an effect on the results of simulation.

We will furthermore look at the Total Vriens model (model 3) and the Implicit Bond-breaking model (model 4), which can be found in figure 4.5 and 4.6 respectively.

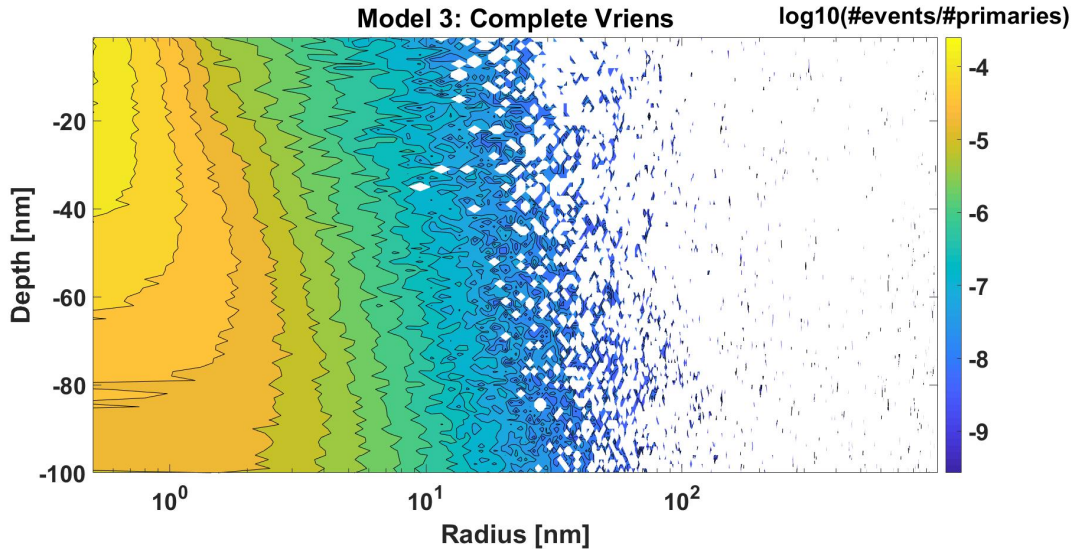


**Figure 4.5:** The normalized bondbreaking effect of the Total Vriens model (model 3). On the horizontal axis, the radius is given on logarithmic scale, and on the vertical axis, the depth is given. The colorscale is logarithmic.

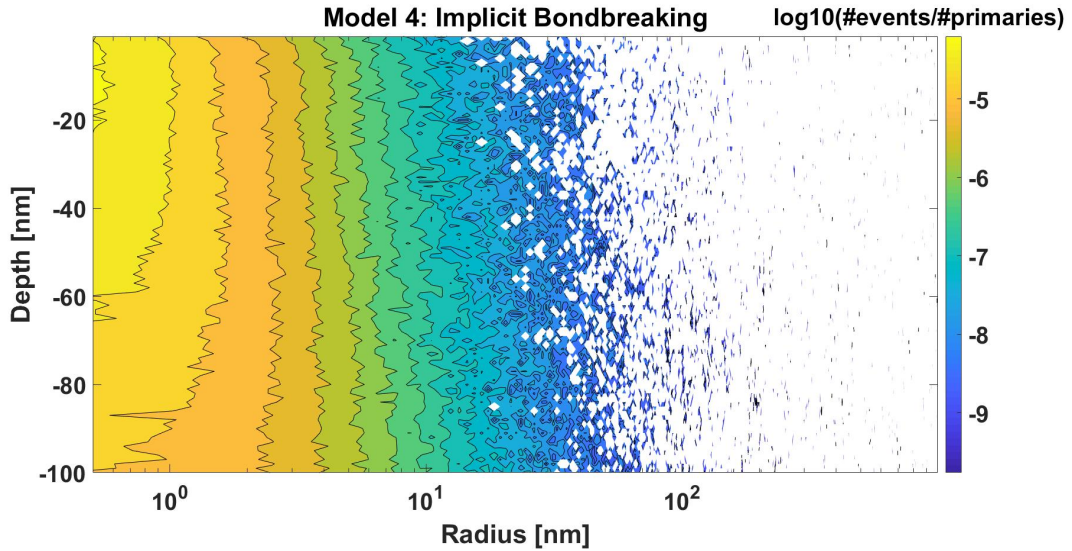


**Figure 4.6:** The normalized bondbreaking effect of the Implicit Bondbreaking model (model 4). On the horizontal axis, the radius is given on logarithmic scale, and on the vertical axis, the depth is given. The colorscale is logarithmic.

The differences between figures 4.5 and 4.6 is given in figure 4.7

It can be seen that the difference between model 3 and 4 is almost constant until a depth of 60nm and a width of 1 nm. This difference is equal to  $10^{0.3} \approx 2$ , which means that in this location, the number of bondbreaking events in the Complete Vriens model is twice as high as the number of bondbreaking events in the Implicit Bondbreaking model.

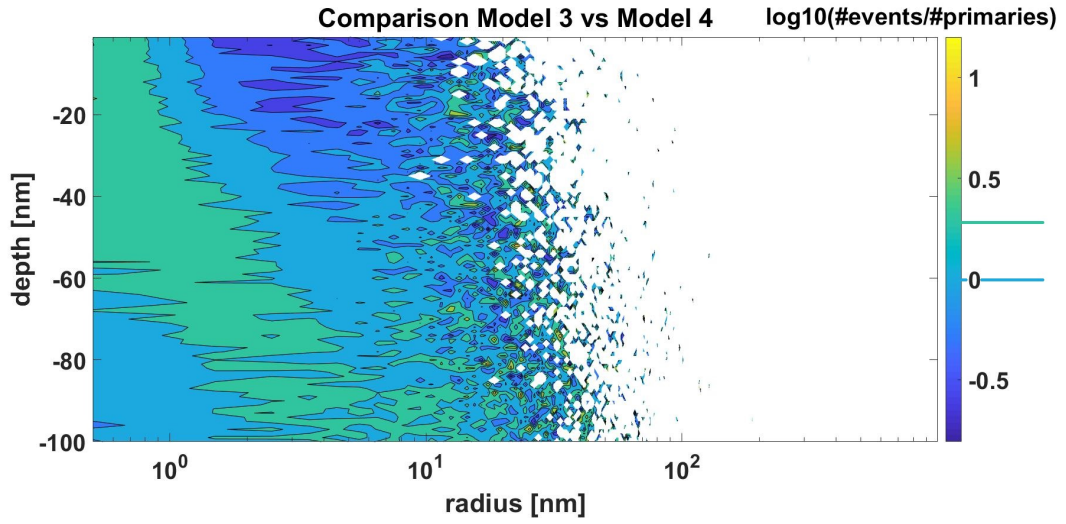


**Figure 4.7:** The difference between the Complete Vriens model (model 3: figure 4.5) and the Implicit Bond-breaking model (model 4:- figure 4.6). On the horizontal axis, the radius is given on logarithmic scale, and on the vertical axis, the depth is given. The colorscale is logarithmic.

Furthermore, we would like to look at the Energy Deposition model (model 5). The radial plot now consists not out of the number of bondbreaking events per bin divided by the bin volume and the total number of primary electrons, but out of the total transferred energy per bin due to inelastic collisions in eV divided by the bin volume and the total number of primary electrons.

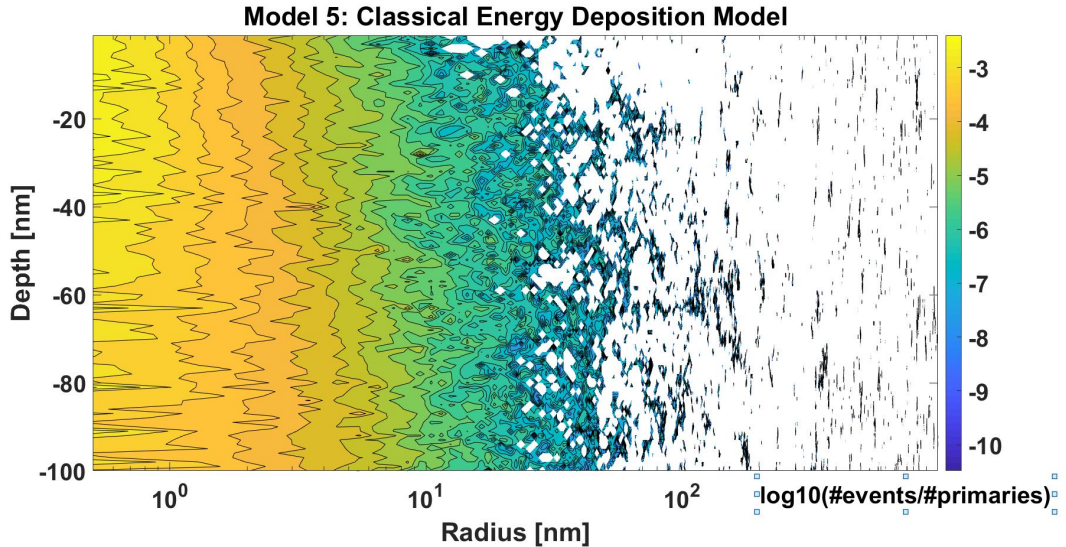


**Figure 4.8:** The normalized transferred energy per cubic nanometer of the Classical Energy Deposition model (model 5). On the horizontal axis, the radius is given on logarithmic scale, and on the vertical axis, the depth is given. The colorscale is logarithmic.

As we can see, 4.8 renders very uncertain results. Therefore we would like improve on it by using a beam of  $1e6$  electrons but only plot it until a radius of 100nm. The 100nm radial border is chosen because bigger borders renders data files of a gigabyte.

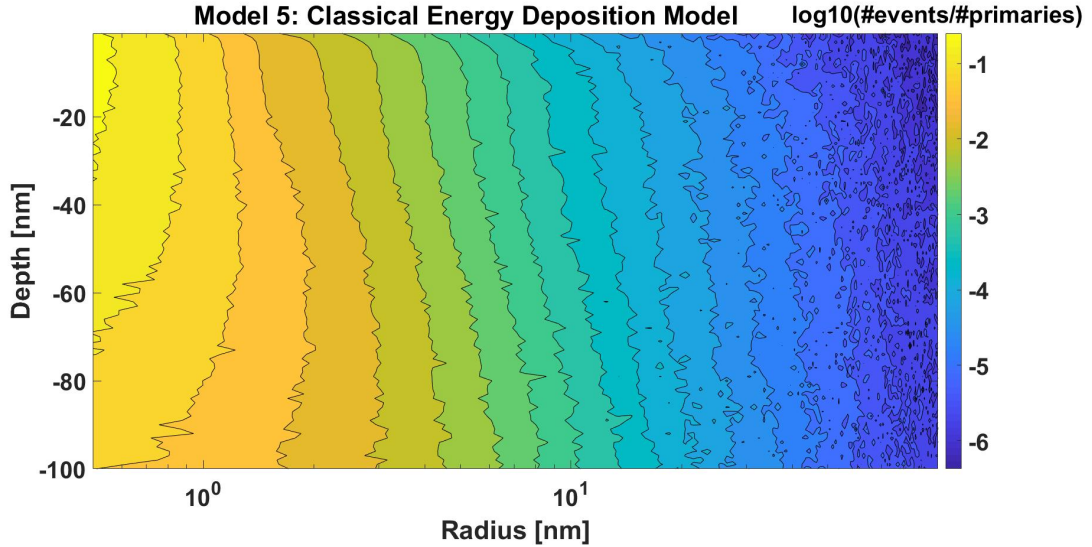


**Figure 4.9:** The normalized transferred energy per cubic nanometer of the Classical Energy Deposition model (model 5). On the horizontal axis, the radius is given on logarithmic scale, and on the vertical axis, the depth is given. The colorscale is logarithmic.

To get a clearer view on the way the different models differ from the Energy Deposition model, we would like to look at figures 4.10, 4.11 and 4.12.

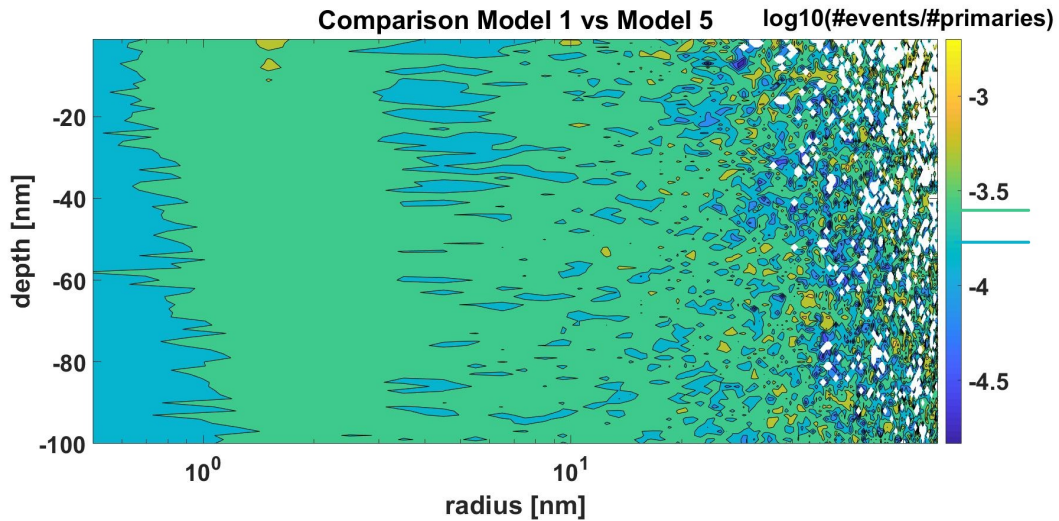


**Figure 4.10:** The difference between figure 4.1 (the Original model) and figure 4.8 (the Energy Deposition model). Or just model 1 vs model 5.

When looking at figures 4.10 to 4.12 we can see that the differences between these

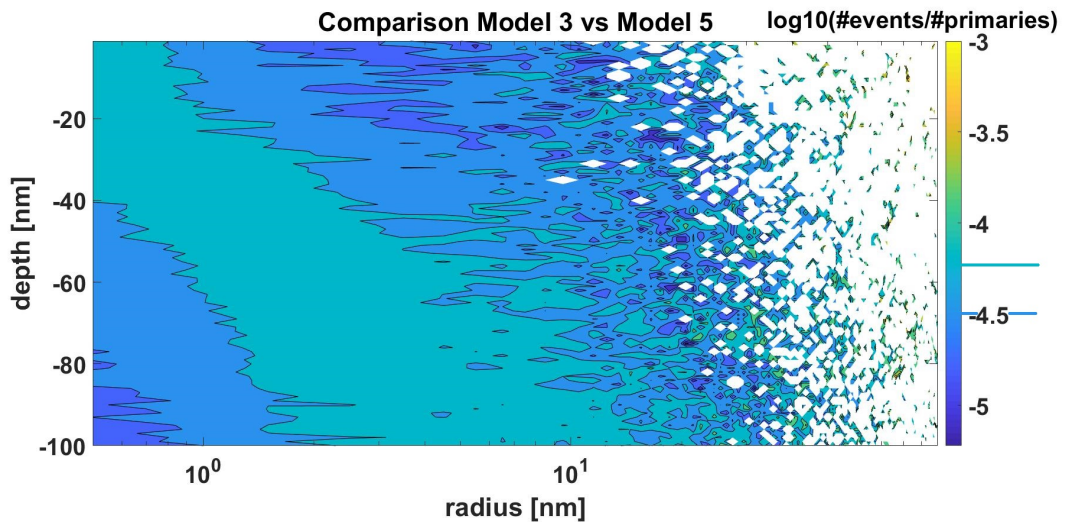


**Figure 4.11:** The difference between figure 4.5 (the Complete Vriens model) and figure 4.8 (the Classical Energy Deposition model). Or just model 3 vs model 5.

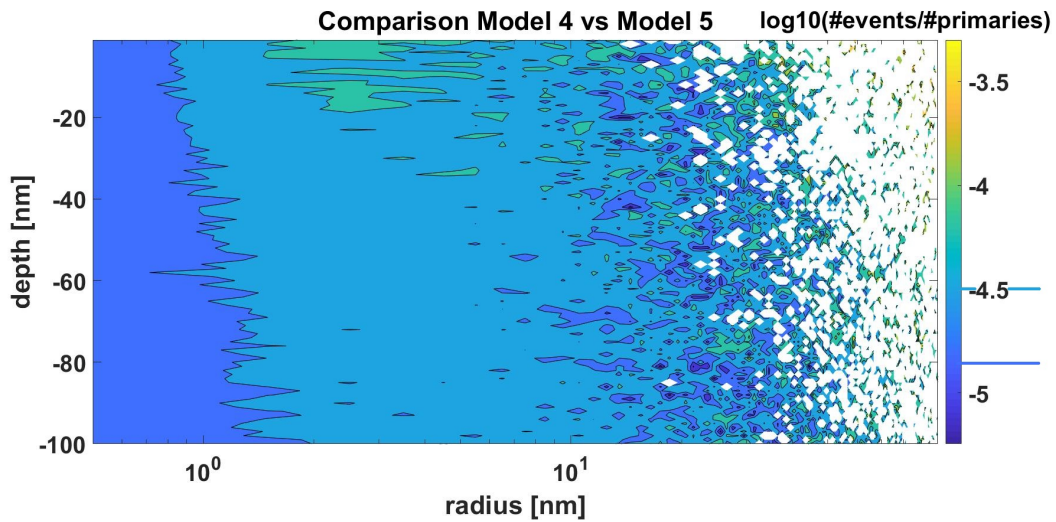


**Figure 4.12:** The difference between figure 4.6 (the Implicit Bondbreaking model) and figure 4.8 (the Classical Energy Deposition model). Or just model 4 vs model 5.

models are almost constant. For model 1 and model 4 (the Original and the Implicit Bond-breaking model), it seems that difference takes somewhat the same shape. For model 3 (Complete Vriens) this shape spreads out and becomes very big. This is probably due to model 3 being more cloud shaped than the other models, which are more shaped in a straight line.

## 4.2.2 The Fraction on Scattering Events

We would also like to take a look at the fraction of scattering events each model yields. For faster programming speed, a beam consisting of a 1,000 electrons on an infinitely small area is used. Again, the resist layer is infinitely deep, which means there is no underlying substrate layer.

**Table 4.1:** The percentage of events per scattering mechanism for each model during simulation. Main-chain is the bondbreaking introduced in this report, adjacent is used to describe the breaking of non main-chain bonds in the complete Vriens model (Model 3 -Complete Vriens). On the right column, the total number of scattering events is given.

	% Main-Chain	% Adjacent	% Inelastic	% Elastic	Total
<b>Model 1:</b> <i>Original</i>	43	-	32	25	2,742,280
<b>Model 2a</b> <i>0.2x Cross section</i>	18	-	41	41	3,862,713
<b>Model 2b:</b> <i>0.5x Cross section</i>	32	-	32	36	3,157,488
<b>Model 3:</b> <i>Complete Vriens</i>	7	66	16	11	1,690,983
<b>Model 4:</b> <i>Implicit Bondbreaking</i>	4	-	41	55	4,492,807
<b>Model 5:</b> <i>Energy Deposition</i>	-	-	44	56	5,480,432

It is interesting to see that model 4 generates a different number of total events than model 5 does, as they are both using only Penn's model. The big difference, however, is that the bondbreaking model is added with its own scattering mechanism. Apparently, using this mechanism one out of ten times when  $\omega > U$ , fewer electrons are generated or electrons lose their energy more quickly. To understand this better, a deeper knowledge into Penn's model is required.

When looking at table 4.1, we mostly see the percentage of the bondbreaking events change in model 1, 2a and 2b. This makes sense as we are changing the cross section which means the probabilities are changed too. It is however interesting to look at the difference between model 3 and 4. If we see the non main-chain bondbreaking events as inelastic events (they generate secondary electrons while not changing the solubility of the material), it can be seen that model 3 has a fraction of inelastic events that is unrealistically large. Even though no clear results can be shown from this, it does show how drastically different model 3 is in comparison to the standard model.

Model 1 and 2b also has a bondbreaking fraction that seems to be too large. Model 4 however renders realistic results when looking at the number of inelastic scattering processes and elastic scattering processes.

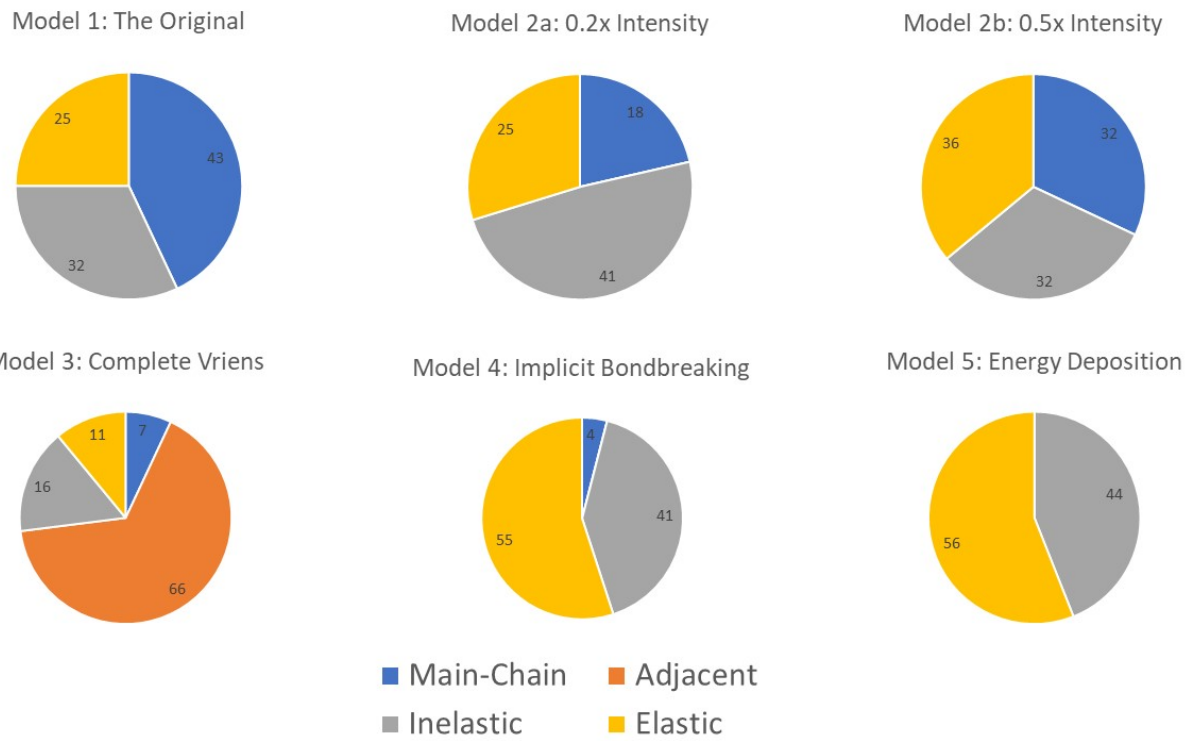


**Figure 4.13:** The percentages of events per model given. The actual numbers can be found in tabel 4.1.

### 4.2.3 Electron Yield

It is also interesting to take a look at the electron yield and the back scattered electron yield. For these calculations, a beam of 1,000 electrons on an infinitely small spot for an infinitely large layer of PMMA are used. The total electron yield is given in figure 4.14a and the back scattered electron yield (BSE-yield) is given in figure 4.14b.

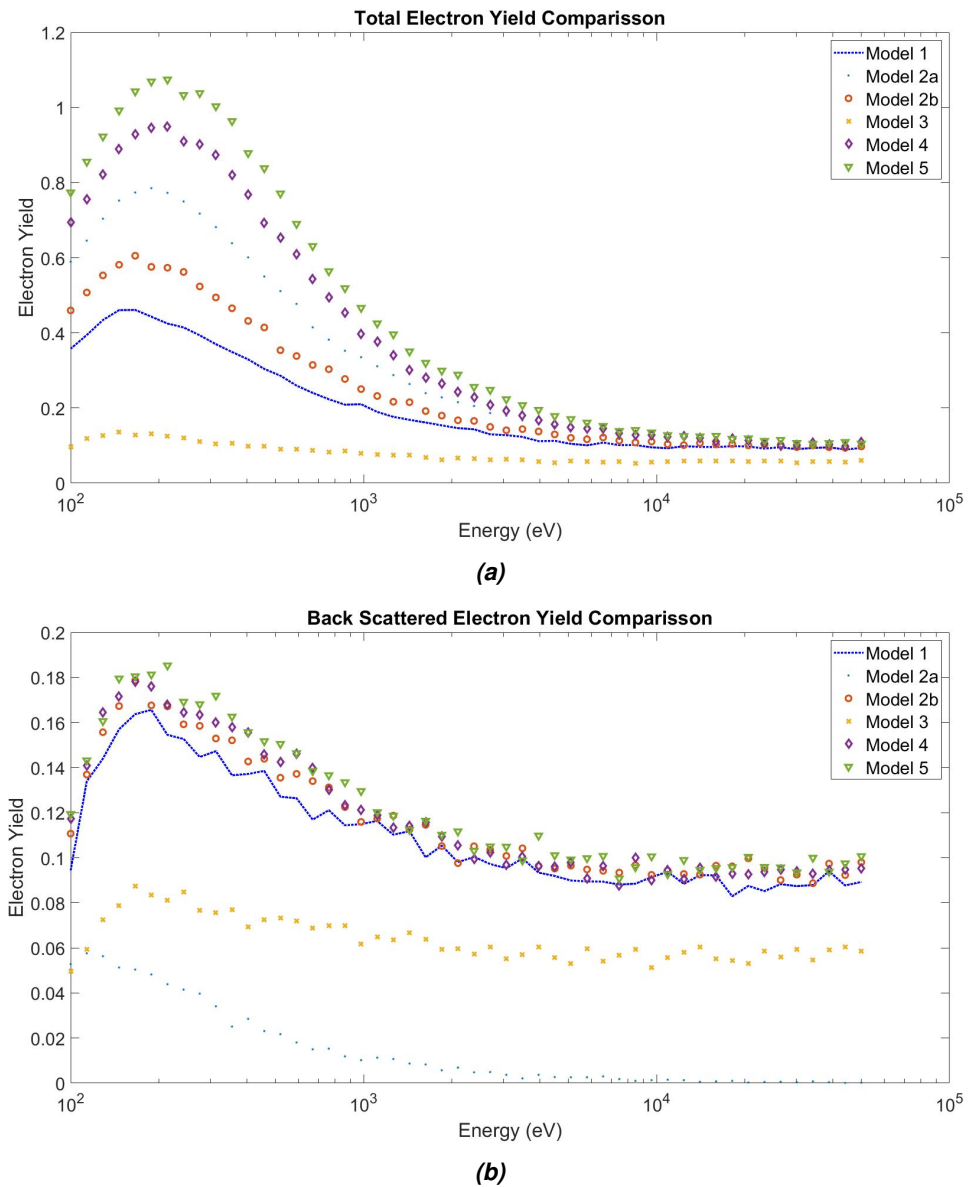


**Figure 4.14:** (a) A comparison of the Electron Yield between all the models. (b) A comparison of the Back Scattered Electron Yield between all the models. Both the yields are plotted vs the logarithmic primary kinetic energy in eV. Experimental data from both Joy and Song<sup>[20]</sup> are included.

When comparing the BSE-yields of figure 4.14b, it seems very obvious that the results

from the model 3 (Complete Vriens model) and model 2a (0.2x Cross section) in the lower energy regime are not in agreement with literature (model 5: Energy Deposition), which we assume to be the correct model. Therefore we can already conclude that model 2a and 3 are incorrect.

When looking at the other models in figure 4.14b, we can see that model 2b (0.5x Cross section) and model 4 (Implicit Bondbreaking) lie a little bit closer to model 5, but as these differences are very small, we cannot conclude anything from it.

When looking at figure 4.14a, we can see that only model 4 renders results in order with model 5. But because we cannot say for sure that model 5 renders the right secondary electron yields, we cannot conclude anything from this model<sup>2</sup>.

One last interesting aspect of figure 4.14b is that model 1 and model 2b lie in the close proximity of model 5, whereas model 2a and model 3 lie way off. This tells us that that small changes in the order of magnitude of the cross section or the number density do not influence the BSE yield by a lot.

We can also compare the BSE and SE yield to some literature values. For this, we will only take the plot ranging from 0 to 35keV. The resulting figures from figure 4.16 are compared to the computed results from Kotera, M. (1999)<sup>[21]</sup> from figure 4.15

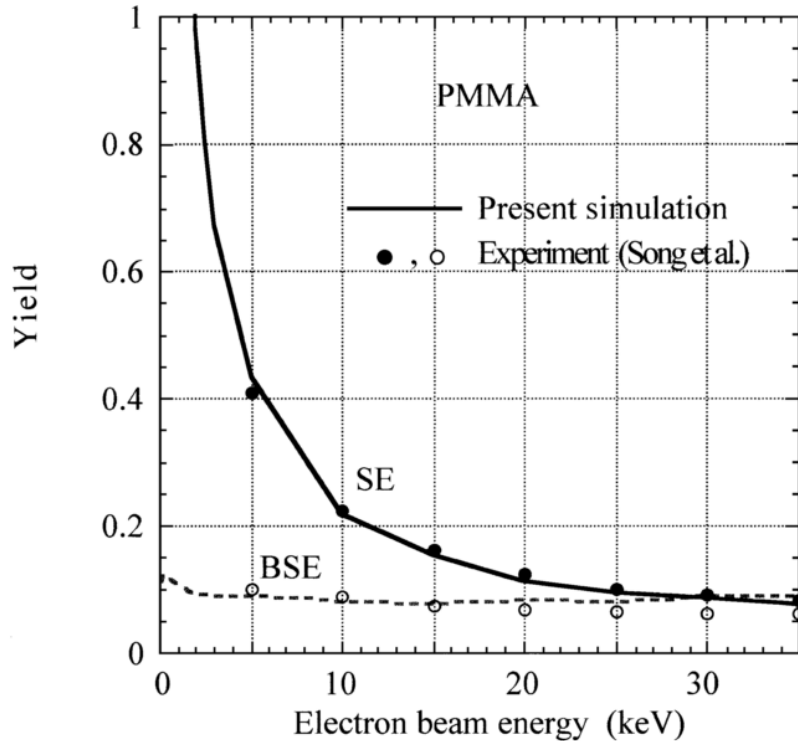


**Figure 4.15:** Computational results from Kotera, M.(1999)<sup>[21]</sup>. A Monte Carlo simulation for the electron trajectories has been done on PMMA and from it these SE and BSE yields are calculated.

---

<sup>2</sup>Penn, D. (1987)<sup>[8]</sup> and Mott, N. (1929)<sup>[9]</sup> are good in calculating the correct BSE yield, but are uncertain in calculating the SEY. Still, figure 4.14a has been included for completeness and further research.

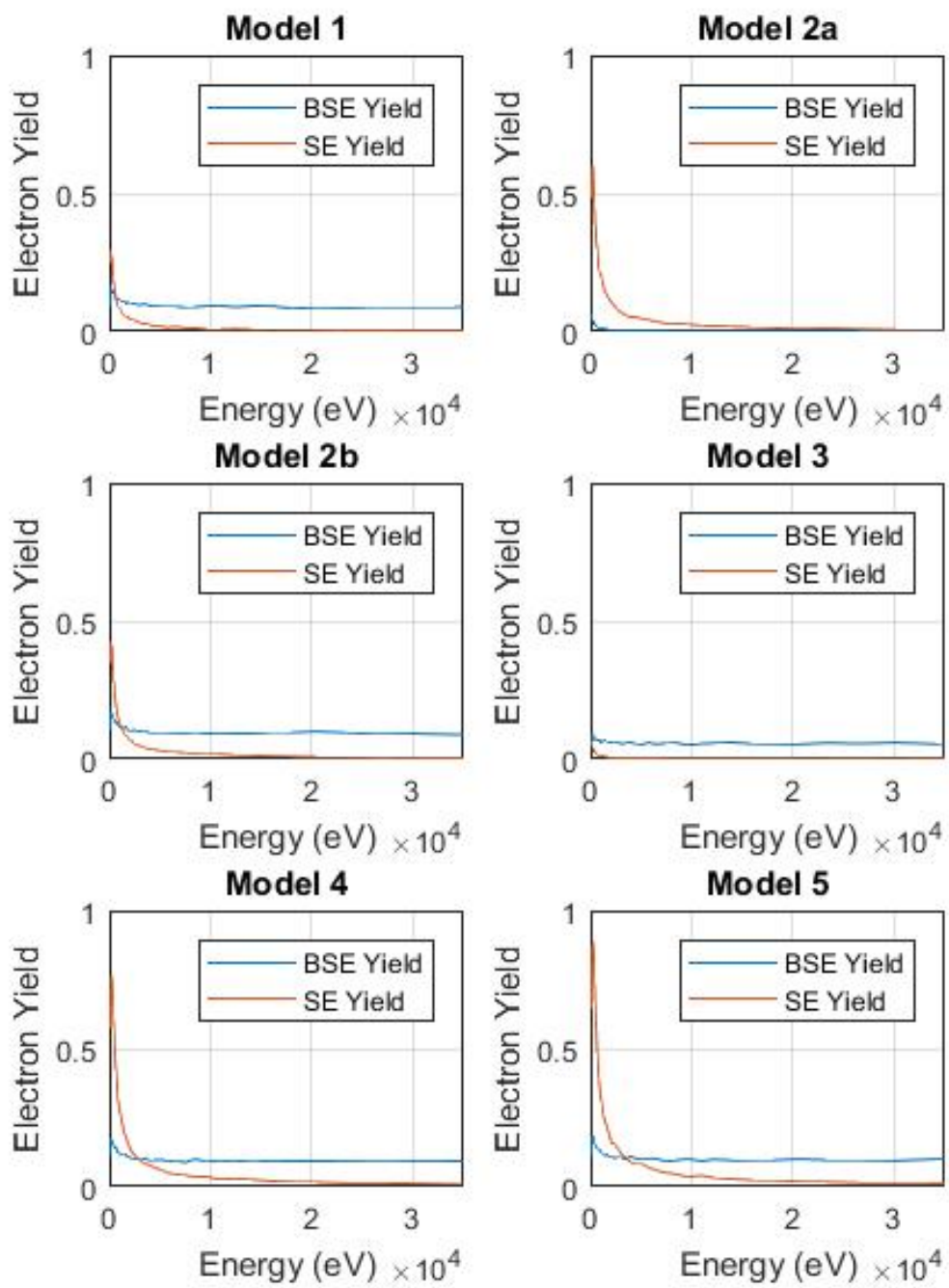


**Figure 4.16:** Comparison between the different BSE and SE yield per model on a linear scale.

If we compare figures 4.16 with 4.15, we see that only model 4 (Implicit Bondbreaking model) and model 5 (Energy Deposition model) render correct SE-yields.

#### 4.2.4 Independent Processes

It can be concluded that every model except model 4 and 5 (Implicit Bondbreaking and Energy Deposition) renders unrealistic results. Furthermore, it is evident that in every category, the Complete Vriens model seems to be the most unrealistic of all the models.

If we consider the Complete Vriens model to be incorrect, it is logical that model 1, 2a and 2b (Original, 0.2x Cross section and 0.5x Cross section) also be wrong, as they are based on the same principle as model 3.

Furthermore, the Implicit Bondbreaking model is only an estimation of an actual model in which bondbreaking would be implemented as part of Penn's inelastic scattering model. Because the estimation still renders better results than actual bondbreaking models based on Vriens as an independent process, we can conclude that bondbreaking should already be part of Penn's inelastic scattering model<sup>3</sup>.

#### 4.2.5 Maximum Number of Broken Bonds

In e-beam lithography, doses of  $150\mu\text{C}/\text{cm}^2$  are used. This translates to 9.4 electrons per squared nanometer. When looking at figure 4.6, we see that a maximum of  $1\text{e-}4$ bonds per cubic nanometer per primary electron are broken, directly at the entrance point. Taking into account the 9.4 electrons per squared nanometer would result in a maximum amount of  $1\text{e-}3$  broken bonds per cubic nanometer, as we see that the number of bondbreaking events decays very quickly. This indicates that the maximum number of 14.1 bonds per nanometer from chapter 3 is never reached.

---

<sup>3</sup>This result can also be backed by figure 4.14b, which seems to indicate model 4 to be slightly better than model 1 or 2b.

# 5 | Discussion and Conclusion

## 5.1 Theory Analysis

In this bachelor project, bondbreaking processes for poly-methylmethacrylate (PMMA) resists have been researched. Starting from main-chain scissions as an indication of the exposed areas of the resists, a bondbreaking model based on classical scattering processes has been developed. This bondbreaking model has been compared to a few other models like the energy deposition model.

Since the bondbreaking model was based on a lot of assumptions, it has a lot of flaws. The list of assumptions can be found in appendix A. Most of the assumptions are already discussed in the theory, but we would like to discuss two of them:

**iv:** *Only direct inelastic collisions with covalent electrons result in bondbreaking. In particular, inner shell excitations and electron trapping effects are ignored.*

Contrary to Aktary, M. (2006)<sup>[13]</sup> and Stepanova, M. (2010)<sup>[14]</sup>, Sun, B. (2014.)<sup>[1]</sup> (figure 13) says that the breaking of adjacent bonds can also result in main-chain scissions due to the monomer changing chemical composition. This effect will result in a number density 3/2 times larger than assumed in this report. As discussed in the results, the shape of the distribution does not change when small changes in the cross section or the number density are made, so this process will not have any notable effects. It is however interesting to see that there are also chemical effects influencing the bondbreaking process.

We also know that there are other mechanisms that can lead to bondbreaking (plasmon excitations, inner shell excitations, etc). Some of these mechanisms are already part of Penn's inelastic model, so it is very probable that ignoring these bondbreaking events inside Penn's inelastic model influence the outcome of our simulation.

**ix:** *PMMA is handled as a metal with the bottom of the conduction band being equal to the Fermi energy.*

In this report, PMMA is used as a metal. This can be seen by first looking at Penn's inelastic model which is based on free electron gasses. The approximation that electrons behave as free electrons is valid for metals, where electrons can flow almost free throughout the material, but doesn't work for insulators like PMMA, where electrons are bound to their molecules. Furthermore, the conduction band is assumed to have its bottom at zero. From this assumption, the Fermi energy is also assumed to be zero. This is also an assumption that might be valid for metals, in which the Fermi energy lies inside the conduction band. For insulators, which the Fermi energy is in the bandgap in between the

valence and the conduction band, this assumption is false. But as calculating the Fermi energy for insulators is very difficult, almost near impossible, a separate study has to be done in order to understand how PMMA would behave different in comparison to metals as resist.

## 5.2 Results Analysis

### Bondbreaking and Penn's Inelastic Model

When reviewing the results, we can first of all say that simulating the bondbreaking model of this report independently of Penn's inelastic model and Mott's elastic model renders an accurate distribution and has a BSE yield that only deviates by a little. It can however be seen that the percentage of broken bonds in relation to the total number of scattering events is very high.

We can also see that implementing the bondbreaking process as part of Penn's inelastic model renders an equivalent distribution to that of the bondbreaking model derived in this report. Furthermore, the BSE yield lies closer to what we expected than the BSE yields calculated in other models, but since this difference is very small we can conclude that both the independent model derived in this report and bondbreaking as part of Penn's model render realistic results.

It is however important to note that the bondbreaking model as derived in this report is based on Vriens' cross section, which was an ionization model meant to be used for all bonds in the material. However, the model derived in this report only used Vriens' cross section for main-chain C-C bonds, ignoring all other bonds PMMA has. Even though this assumption rendered realistic results, it is wrong on a theoretical basis. Furthermore, we have proven that by using the right assumption by taking all bonds inside PMMA into account in Vriens' cross section renders unrealistic results.

Bondbreaking as part of Penn's inelastic model was only approximated in this report but still rendered similar realistic results as our bondbreaking model. Since this is an approximation but has a much better theoretical basis, using bondbreaking as part of Penn's inelastic model seems preferable to using the bondbreaking model derived in this report.

### Bondbreaking and Inelastic Energy Deposition Model

Another interesting result is that the classic inelastic energy deposition model also renders results which seem to be in order with both the bondbreaking model implemented separately and the bondbreaking model implemented as part of Penn's inelastic model. There are however still some differences, but as these are very small we can conclude that using a separate bondbreaking model has no advantages over the energy deposition model, at least until a better bondbreaking model has been developed.

### 5.3 Recommandations

For further research, a more detailed investigation into Penn's inelastic model and the underlying dielectric function needs to be done. We are mostly interested in how bond-breaking and Penn's inelastic model are related. When looking at paragraph 3.3, we see that Vriens cannot be completely part of Penn. In paragraph 5.2, on the other hand, we discovered that bondbreaking is most likely part of Penn's inelastic model. It might be possible that Vriens' cross section is wrong and we only need to focus on Penn's inelastic model, but it might also be possible that some parts of Vriens are already contained in Penn. To investigate this further, a deeper understanding in the quantum mechanics behind both the bondbreaking process as well as Penn's inelastic model is needed.

It is also interesting to look at the effects bondbreaking has on the overall material from a chemical point of view. Chemical reactions may have a big effect per bond broken depending on which material resist is used. We already know about cross linking and different ways bondbreaking can happen. These effects can be researched further and also be implemented in the theory.

We also know that a lot of assumptions are based on the solid state theories for metals. Since we are interested in PMMA, a big improvement would be to adjust these assumptions to make it fitting for insulators as well. As this is hard to research the solid state aspects of insulators and very little literature about it is known, PMMA itself probably needs to be researched.

Aktary, M. (2006)<sup>[13]</sup> and Stepanova, M. (2010)<sup>[14]</sup> goes a little bit deeper into the cross section and also uses Gryzinski's cross section<sup>[4,5]</sup>. Aktary also calculates the stopping power of the model. This calculated stopping power is also compared to its empirical equivalent, from which a few fitting parameters are calculated. In this report, no comparison is made using the stopping power. And since it made a big difference in Aktary it might be interesting to look into it. Furthermore, some empirical data surrounding the BSE yield would also render more accurate results.

### 5.4 Conclusion

Most importantly, it can be concluded that including a separate bondbreaking model in our simulation renders no better results than using the inelastic deposition model. Adding bondbreaking as a process independent from Penn's inelastic model has proven itself to lead to unrealistic backscatter yield. The model derived in this report ignores adjacent molecules, which renders realistic results, but is not self-consistent.

Implementing bondbreaking as part of Penn's inelastic model however has rendered equivalently realistic results, but seems to be more self-consistent. In this report, bond-breaking has only been implemented as a very rough estimation by making it a random chance process based on the total amount of bonds in the material, so this model can be improved a lot.

In further research, it would be interesting to look at how bondbreaking can be implemented as part of Penn's inelastic model in a more physically accurate way. For this, a deep research into Penn's inelastic model and the underlying dielectric function needs

to be done. Furthermore, the bondbreaking mechanism of this paper can be improved a lot more by looking at it from both a more quantum mechanical way, but also from a chemical point of view.

As last, a lot could be improved by making Penn's inelastic model also fit the aspects of an insulator, as it is now primarily based on metals.

## A | Assumptions of the model

- i The material does not contain impurities which may affect the bondbreaking process.
- ii The effect of cross linking between ionized polymers is negligible/broken bonds do not reconfigure.
- iii Each polymer chain is in the order of thousands carbon atoms long and varies largely in length.
- iv Only directly breaking a main-chain C-C bond will result in a main-chain scission. Furthermore, only main-chain scissions result in a notable change in solubility in PMMA/Breaking of adjacent bonds do not result in a change in the material.
- v The binding energy of the main-chain C-C bonds is equal to 4.9eV from Wu's paper<sup>[7]</sup>.
- vi Only direct inelastic collisions with covalent electrons result in bondbreaking. In particular, inner shell excitations and electron trapping effects are ignored.
- vii The binding energy U disappears and has no effect on the material or further scattering events.
- viii Relativistic effects can be neglected.
- ix PMMA is handled as a metal with the bottom of the conduction band being equal to the Fermi energy.
- x Electrons at the bottom of the conduction band are free but have no kinetic energy, so  $E_F = 0$ .
- xi The azimuthal angle is chosen from a uniform  $U(0,2\pi)$  distribution. The polar angle follows a distribution derived from Vriens' cross section.
- xii The transferred energy must be bigger than the binding energy in order to break the bond.
- xiii The maximum number of broken bonds is never reached and effects of charging are ignored/the material stays unchanged. Therefore, there is no need to change the simulation during simulation. This also means density changes due to shrinkage effects are ignored.

- xiv Vriens' ionization cross section and Penn's inelastic model are independent processes and therefore, bondbreaking and inelastic scattering are independent processes. (*specific for the model derived in this report only.*)
- xv Model 3 assumes an uniform binding energy of 4.9eV for each bond in PMMA.
- xvi Vriens' cross section is correct at all energies
- xvii Penn's inelastic model is correct at all energies
- xviii The elastic cross section (Mott scattering + transition to phonon at low energy, see<sup>[18]</sup>) is correct at all energies.

# Bibliography

- [1] Bo Sun. Low-energy electron-induced chemistry of PMMA. (July):1–43, 2014.
- [2] C. Vieu, F. Carcenac, A. Pépin, Y. Chen, M. Mejias, A. Lebib, L. Manin-Ferlazzo, L. Couraud, and H. Launois. Electron beam lithography: Resolution limits and applications. *Applied Surface Science*, 164(1-4):111–117, sep 2000.
- [3] Vitor R. Manfrinato, Lihua Zhang, Dong Su, Huigao Duan, Richard G. Hobbs, Eric A. Stach, and Karl K. Berggren. Resolution limits of electron-beam lithography toward the atomic scale. *Nano Letters*, 13(4):1555–1558, 2013. PMID: 23488936.
- [4] Michał Gryziński. Two-particle collisions. I. General relations for collisions in the laboratory system. *Physical Review*, 138(2A), 1965.
- [5] Michał Gryziński. Two-particle collisions. II. Coulomb collisions in the laboratory system of coordinates. *Physical Review*, 138(2A), 1965.
- [6] L. Vriens. Binary-encounter electron-atom collision theory. *Physical Review*, 141(1):88–92, 1966.
- [7] Bo Wu and Andrew R. Neureuther. Energy deposition and transfer in electron-beam lithography. *Journal of Vacuum Science & Technology B: Microelectronics and Nanometer Structures*, 19(6):2508, 2001.
- [8] David R. Penn. Phys. Rev. B 1987 Penn Electron mean-free-path calculations using a model dielectric function.pdf. *Physical Review*, 35(2), 1987.
- [9] N.F. Mott. Scattering o f Fast Electrons by Atomic Nuclei. *Proc. R. Soc. A*, 124:425, 1929.
- [10] N E W Youth and Views Sustainability. PMMA, from plexiglass window to a packaging for an implantable glu- cose sensor. (June):16–18, 2015.
- [11] Daniel J Carbaugh, Jason T Wright, Rajan Parthiban, and Faiz Rahman. Photolithography with polymethyl methacrylate (PMMA). *Semiconductor Science and Technology*, 31(2):025010, 2016.
- [12] Umar Ali, Khairil Juhanni Bt Abd Karim, and Nor Aziah Buang. A Review of the Properties and Applications of Poly (Methyl Methacrylate) (PMMA). *Polymer Reviews*, 55(4):678–705, 2015.

- [13] M. Aktary, M. Stepanova, and S. K. Dew. Simulation of the spatial distribution and molecular weight of polymethylmethacrylate fragments in electron beam lithography exposures. *Journal of Vacuum Science & Technology B: Microelectronics and Nanometer Structures*, 24(2):768, 2006.
- [14] M. Stepanova, T. Fito, Zs. Szabó, K. Alti, A. P. Adeyenuwo, K. Koshelev, M. Aktary, and S. K. Dew. Simulation of electron beam lithography of nanostructures. *Journal of Vacuum Science & Technology B, Nanotechnology and Microelectronics: Materials, Processing, Measurement, and Phenomena*, 28(6):C6C48–C6C57, 2010.
- [15] Marcia C.K. Tinone, Kenichiro Tanaka, Junya Maruyama, Nobuo Ueno, Motoyasu Imamura, and Nobuyuki Matsubayashi. Inner-shell excitation and site specific fragmentation of poly(methylmethacrylate) thin film. *The Journal of Chemical Physics*, 100(8):5988–5995, 1994.
- [16] L. Vriens. Electron exchange in binary encounter collision theory. *Proceedings of the Physical Society*, 89(1):13–21, 1966.
- [17] cstool. <https://github.com/eScatter/cstool>, 2017. Cross Section Tool, T. Verduin, TU Delft.
- [18] Thomas Verduin. *Quantum Noise Effects in e-Beam Lithography and Metrology*. TU Delft, 2017.
- [19] Matlab r2018a - academic use, 2018. The MathWorks, Natick, MA, USA.
- [20] David C Joy. ELECTRON-SOLID INTERACTIONS Compiled by. *A Database of Electron Solid Interactions*, (April):334, 2008.
- [21] Masatoshi Kotera, Kiyoshi Yamaguchi, and Hiroshi Suga. Dynamic simulation of electron-beam-induced chargingup of insulators. *Japanese Journal of Applied Physics*, 38(12S):7176, 1999.